

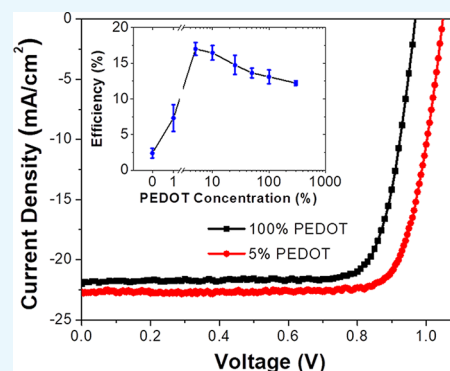
Ultrathin Hole Extraction Layer for Efficient Inverted Perovskite Solar Cells

Dianyi Liu,[†] Qiong Wang,^{‡,||} Mark Elinski,[†] Pei Chen,[†] Christopher J. Traverse,^{†,⊥} Chenchen Yang,[†] Margaret Young,^{†,¶} Thomas W. Hamann,[‡] and Richard R. Lunt^{*,†,§}

[†]Department of Chemical Engineering and Materials Science, [‡]Department of Chemistry, and [§]Department of Physics and Astronomy, Michigan State University, East Lansing, Michigan 48824, United States

Supporting Information

ABSTRACT: Inverted perovskite solar cells (PSCs) incorporating poly(3,4-ethylenedioxythiophene)–poly(styrenesulfonate) (PEDOT) as the hole transport/extraction layer have been broadly investigated in recent years. However, most PSCs which incorporate PEDOT as the hole transport layer (HTL) suffer from lower device performance stemming from reduced photocurrent and low open-circuit voltage around 0.95 V. Here, we report an ultrathin PEDOT layer as the HTL for efficient inverted structure PSCs. The transparency, conductivity, and resulting film morphology were studied and compared with traditional architectures and thicker PEDOT layers. The PSC device incorporating an ultrathin PEDOT layer shows significant improvement in short-circuit current density (J_{SC}), open-circuit voltage (V_{OC}), and power conversion efficiency. Because ultrathin PEDOT layers can be easily obtained by dilution, this study suggests a simple way to improve the PSC performance and provide a route to further reduce the fabrication complexity and cost of PSCs.



1. INTRODUCTION

Perovskite solar cells (PSCs) have made substantial progress as competitive photovoltaic candidates in recent years.^{1–7} The power conversion efficiency (PCE) of PSCs has significantly improved from 3.8 to 22.7%.^{1,8} The fast rise of device performance is attributed to the simplification of the device architecture,^{6,9–12} the improvement of processing for absorber materials, and the development of efficient charge selective materials.^{3,9,10,13–16} Additionally, a range of electron- and hole-transporting materials are helping to drive improved PSC performance.^{4,9–11,17} To date, the highest efficiency PSCs with PCE over 20% utilize 2,2',7,7'-tetrakis(*N,N*-di-*p*-methoxyphenylamine)-9,9'-bifluorene (spiro-OMeTAD) or poly(bis(4-phenyl)(2,4,6-trimethylphenyl)amine) (PTAA) as the hole transport layer (HTL).^{3–5,8,10,13,18} Though these types of HTLs exhibit efficient hole extraction and result in attractive device performance, the cost of these materials is especially high compared with the perovskite active layer. In addition, a set of complex additives is required to improve the film conductivity when using these types of HTLs, which increases the processing complexity and reduces yield, repeatability, and reliability.^{7,8}

Poly(3,4-ethylenedioxythiophene):poly(styrenesulfonate) (PEDOT) is a common and low-cost HTL material which is broadly used in the organic electronics field.^{19,20} PEDOT was first introduced in PSCs in 2013 and has since become a popular HTL in inverted structure PSCs because of its flexibility, low-temperature processability, and ease of fabrication.^{11,21} However, most PSCs using PEDOT as the HTL suffer

from lower device performance when compared with the devices using spiro-OMeTAD or PTAA as the HTL.²² The low performance of PEDOT in PSCs are attributed to the moderate conductivity, parasitic absorption, less suitable work function, and the influence of pH in the PEDOT precursor solution.^{23–26} To overcome these disadvantages of pristine PEDOT and improve the device performance, previous work has focused on modification of the film work function and surface properties.^{24–26} For example, Zhu et al. treated PEDOT films with dimethylformamide (DMF) and other organic solvents to enhance the conductivity, which led to an increase in performance from 16.69 to 18.02%.²³ Jen and et al. reported that the modulation of PEDOT pH could reduce the device potential loss and enhance the device open-circuit voltage (V_{OC}) from 0.88 to 1.06 V.²⁴ Zuo and Ding adjusted the polystyrene sulfonate content in PEDOT precursors to change the work function of PEDOT, transmittance, charge carrier extraction capability, and film morphology.²⁶ It was also reported that hybrid or functionalized PEDOT films can lead to high efficient PSCs.^{22,27,28}

In this work, we demonstrate the influence of the PEDOT film thickness on the photovoltaic performance of PSCs in an inverted structure. We employ an ultrathin PEDOT film (2 nm) as the HTL in PSCs without the need for additional processing steps and show that the device PCE can be

Received: April 18, 2018

Accepted: May 25, 2018

Published: June 13, 2018

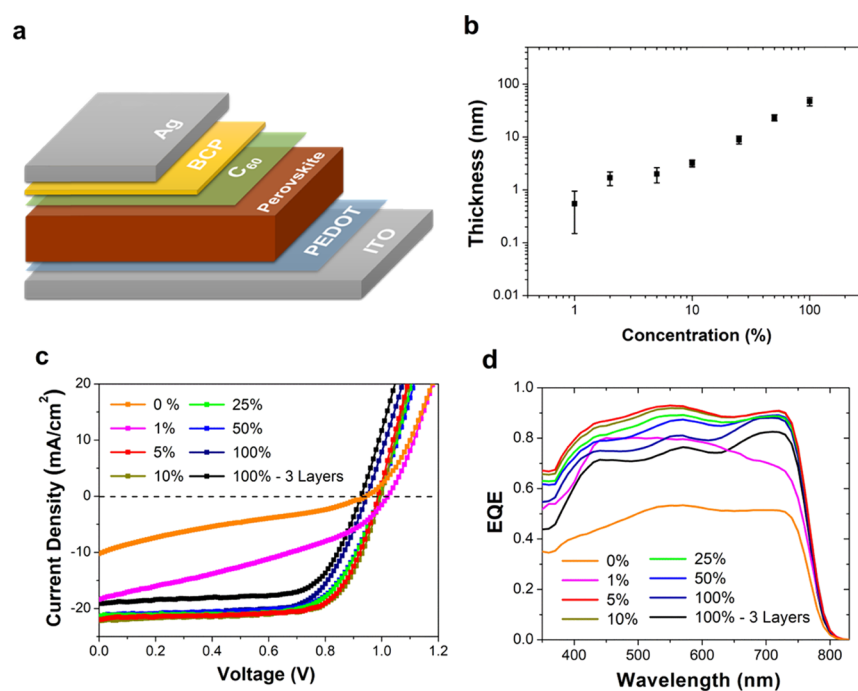


Figure 1. (a) Device architecture. (b) PEDOT film thickness as a function of the concentration of PEDOT precursor solution. (c) Current density–voltage (J – V) curves of PSCs prepared with various concentrations of PEDOT precursor solutions. (d) Corresponding EQE spectra of the perovskite devices.

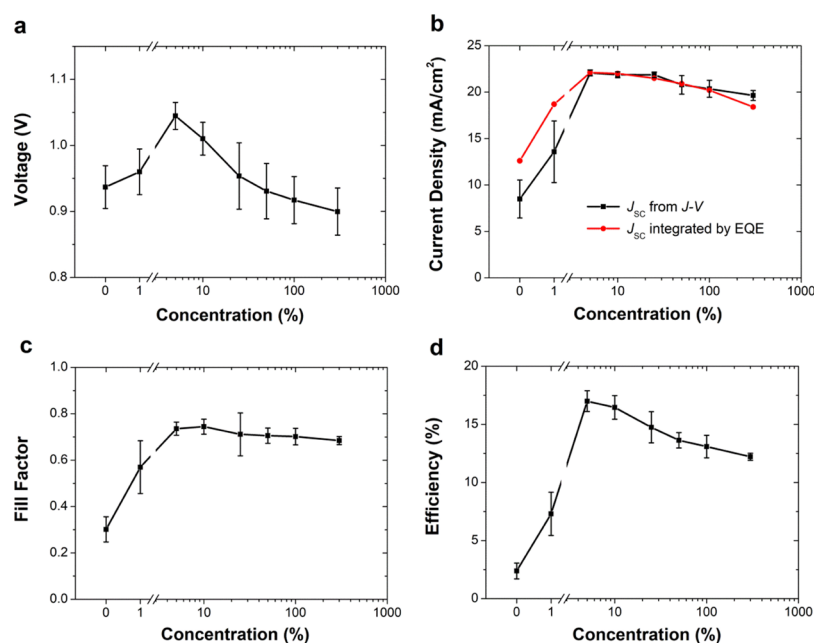


Figure 2. (a) Open-circuit voltage (V_{OC}), (b) short-circuit current density (J_{SC}), (c) FF, and (d) PCE as a function of the concentration of PEDOT solution.

significantly enhanced from 16.9 to 19.3%. The ultrathin PEDOT film is prepared by direct dilution of the PEDOT precursor solution allowing the formation of films as thin as 0.5 nm. The transparency, conductivity, and film morphology of the ultrathin PEDOT layer were studied and compared with thick PEDOT layers. The results suggest that ultrathin PEDOT layers have unique advantages over thick PEDOT films when used as HTLs in PSCs.

2. RESULTS AND DISCUSSION

To probe the influence of PEDOT on the device performance, a batch of devices with various thicknesses of PEDOT were prepared by varying the concentration of the PEDOT solution. Solar cells were fabricated on indium tin oxide (ITO) substrates with the device structure ITO/PEDOT/CH₃NH₃PbI_{3-x}Cl_x (~320 nm)/C₆₀ (20 nm)/BCP (7.5 nm)/Ag (Figure 1a). To measure the film thickness, the PEDOT layer was deposited on precleaned silicon wafer substrates by spin-coating, and then, the thicknesses were measured by spectroscopic ellipsometry. As

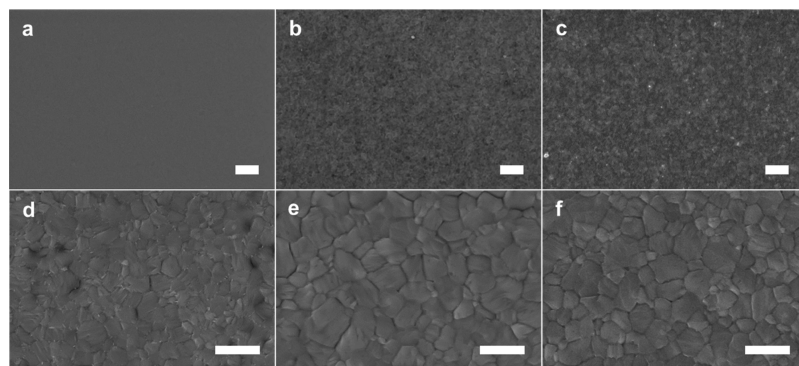


Figure 3. Top-view SEM images of substrates (a–c) and perovskite films (d–f) deposited on each substrate. (a,d) 100%-PEDOT film on ITO. (b,e) 5%-PEDOT film on ITO. (c,f) ITO-only. The scale bar is 1 μm .

seen from Figure 1b, the thickness of PEDOT layer is found to change linearly with the concentration of the original PEDOT solution. The thickness is decreased from 47 ± 8.4 to 0.6 ± 0.4 nm when the PEDOT solution is diluted from 100% (original concentration) to 1%. The perovskite film was then prepared on the PEDOT layer by the vacuum-assist method.²⁹ An electron extraction layer (C_{60}) with the cathode interfacial layer (BCP) was subsequently deposited on top of the perovskite film, and a silver top electrode was deposited by thermal evaporation to complete the device fabrication. Figure 1c shows the current–voltage (J – V) characteristics of the PSCs. A reference device with a thick (116 ± 10.6 nm) PEDOT layer was also fabricated to understand the higher thickness influence on device performance. In addition, a HTL-free (ITO-only) device was also prepared to compare with the ultrathin PEDOT layer device. Figure 1d shows the external quantum efficiency (EQE) of the devices.

The solar cell parameters including the short-circuit current density (J_{SC}), V_{OC} , fill factor (FF), and PCE are plotted as a function of PEDOT concentration in Figure 2. All parameters are gradually enhanced as the PEDOT concentration decreases from 100 to 5%. The 5%-PEDOT device with 2.0 ± 0.6 nm thickness of PEDOT shows the highest PCE. When the PEDOT concentration further decreases to 1%, all of device parameters show a sharp drop. Because the thickness of the 1%-PEDOT layer is less than 1 nm, the extremely thin layer does not form a completely continuous film. This is similar to the ITO-only device performance. In contrast, the ultra-thick-PEDOT device also shows comparable FF, but the J_{SC} and V_{OC} are lower than those of the original PEDOT device. We deduce that the loss of J_{SC} and V_{OC} are also induced by charge recombination. For the device with the thickest PEDOT layer (>100 nm), holes cannot efficiently transfer from the perovskite film to the ITO electrode. Thus, the J – V results clearly indicate that the thickness of the PEDOT layer is a crucial factor for the device performance.

We note that the integrated photocurrent from the EQE spectra is in good agreement with the trend of device J_{SC} (Figures 1d and 2b). The EQE spectra increase when the PEDOT concentration is diluted from 100 to 5%. Further dilution of the PEDOT solution leads to a drop in the EQE. The initial EQE enhancement with decreasing PEDOT concentration is in good agreement with the transparency enhancement across the visible spectrum. The transmission spectra of PEDOT with varying thickness are shown in Figure S1. While the lowest thickness of PEDOT has the highest transparency, the charge recombination and current leakage

more than offset the contribution of the increased light harvesting. For the ITO-only device, the lack of the hole extraction layer leads to an increased recombination at the perovskite film interface and results in a low EQE as well as low J_{SC} .

To further investigate the effect of the ultrathin PEDOT in PSCs, the perovskite film and device on the 100%-PEDOT layer and the 5%-PEDOT layer were studied with scanning electron microscopy (SEM), X-ray diffraction (XRD), ultraviolet photoelectron spectroscopy (UPS), photoluminescence (PL), and impedance spectroscopy. The morphologies of the ITO substrate studied by SEM are shown in Figures 3a–c. When the thickness of the PEDOT film is over 40 nm, we do not observe the underlying ITO morphology. In contrast, the 5%-PEDOT layer is more transparent and the bottom ITO substrate morphology can clearly be observed through the thin PEDOT layer. The low resistance of the ultrathin PEDOT layer not only ensures the holes efficiently transport from the perovskite film to the ITO electrode but also decreases the device series resistance that results in enhanced device performance. The SEM images of perovskite films prepared on PEDOT/ITO substrates (Figure 3d–f) show that the films are homogeneous, continuous, and smooth, and the perovskite films are fully covered on the substrate with few observable pinholes. It should be noted that the grain size of the perovskite film on the 5%-PEDOT layer is clearly larger than the 100%-PEDOT film.

Because the surface properties influence the morphology of the perovskite film, the surface energies of the 5%-PEDOT film and 100%-PEDOT film were evaluated by contact angle measurements (Figure S2).³⁰ These results show the 5%-PEDOT film has a larger water contact angle than the 100%-PEDOT film, which suggests that the grain size of the perovskite film on the 5%-PEDOT layer should be larger than the 100%-PEDOT perovskite film. This phenomenon is in good agreement with the previous report by Huang's group.³⁰ The 5%-PEDOT film with the lowest wetting substrate surface can act to promote the formation of larger perovskite grain size.

The properties of the perovskite films were also characterized by powder XRD. The XRD spectra are shown in Figure S3. The peak intensity of the 5%-PEDOT perovskite film presents the strongest XRD signal compared with the perovskite film on 100%-PEDOT and ITO directly. This again indicates the greater potential for larger grain size and good crystallization with the 5%-PEDOT perovskite film over the 100%-PEDOT perovskite film. The high quality of the perovskite films with

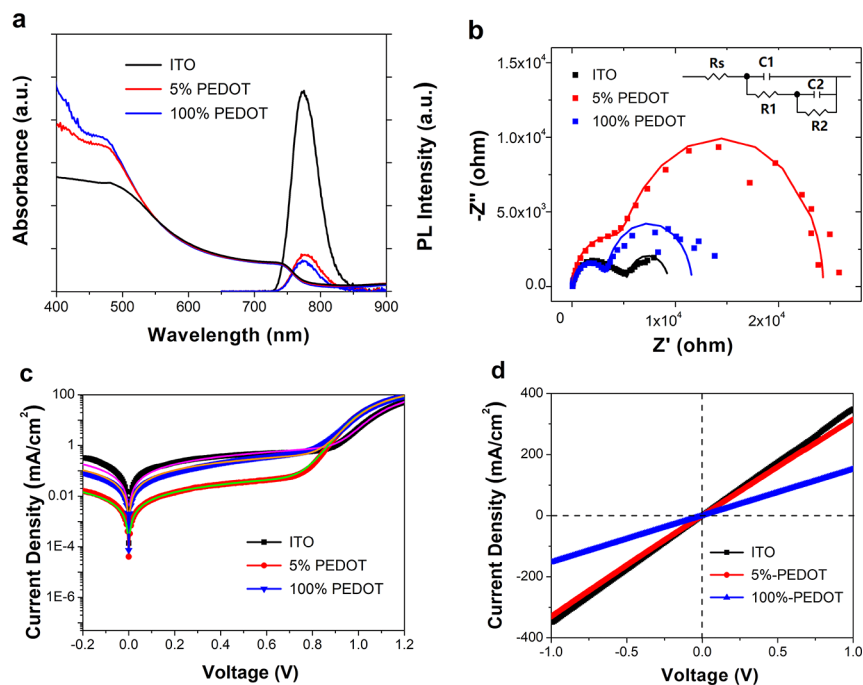


Figure 4. (a) PL spectra for the perovskite films deposited with various thicknesses of PEDOT on ITO substrates. (b) Nyquist plots for the PSCs prepared with various substrates, as measured under 0.1 sun irradiation condition at 0.6 V bias. The inset is the equivalent circuit employed to fit the Nyquist plots. (c) Dark J – V curves of devices with various thicknesses of PEDOT. The solid line is the fitting curve for each dark J – V curves. (d) J – V curves of ITO/PEDOT/MoO₃ (20 nm)/Ag devices for measuring variations in conductivity.

Table 1. Fitting Parameters for Electrochemical Impedance Spectroscopy Data Acquired under 0.1 sun Irradiation Condition with 0.6 V Bias

concentration of PEDOT	R_s (Ω)	R_1 (Ω)	C_1 (F)	R_2 (Ω)	C_2 (F)	t_2 (s)
w/o	68.3	2.14×10^3	7.53×10^{-8}	3.99×10^3	3.46×10^{-6}	1.38×10^{-2}
5%	76.4	6.35×10^3	3.38×10^{-9}	1.73×10^4	2.3×10^{-8}	3.97×10^{-4}
100%	67.3	3.33×10^3	4.07×10^{-9}	8.59×10^3	1.78×10^{-7}	1.53×10^{-3}

larger grain size and improved crystallization can significantly improve the charge transport ability.³⁰

To understand the impact of various thicknesses of the PEDOT layer on the transparent electrode surface, the work functions of bare ITO and ITO/PEDOT layers were characterized by UPS. As shown in Figure S4, the work functions of the 5%-PEDOT layer and the 100%-PEDOT layer are determined to be 5.1 and 5.0 eV, respectively, from the high binding energy cutoff. In contrast, the bare ITO shows a work function of 4.8 eV. The increase of work function (0.1 eV) reduces the energy barrier for hole extraction from the perovskite film to the PEDOT layer, and an improved built-in potential that results in an improved V_{OC} of the 5%-PEDOT device. The improved crystallization of perovskite films discussed above is also expected to contribute the higher V_{OC} of the device.³⁰

Figure 4a shows the absorbance and PL spectra for perovskite films on various substrates. The strong and uniform absorption of all perovskite films in the range of 400–800 nm indicate the high quality and good light harvesting ability of each of the perovskite films. The steady-state PL intensity of the perovskite film on bare ITO substrate is found to be much stronger than the film on the 100%-PEDOT layer. This phenomenon is consistent with the previous report by the Snaith group.²¹ A PL quenching ratio of 85% is found for the 100%-PEDOT layer, which is similar to the quenching ratio of 82% for the 5%-PEDOT layer. The result indicates that the thin

5%-PEDOT layer is sufficient to efficiently extract holes from the perovskite film. While increasing the PEDOT thickness can slightly enhance the hole transfer efficiency, this effect is compensated by increased device series resistance.

To further study the effect of the PEDOT layer on device performance, we performed impedance measurements for each of the devices.³¹ The Nyquist plot of the devices measured under 0.1 sun illumination at 0.6 V forward bias is given in Figure 4b. The equivalent circuit used to model the Nyquist plot is also given in Figure 4d. The parameters extracted from the equivalent circuit are summarized in Table 1. It is clear that the recombination resistance (R_2) of the 5%-PEDOT device is double that of the 100%-PEDOT device, but the residual charge (C_2) of the 5%-PEDOT device is an order of magnitude lower than the 100%-PEDOT device providing an additional explanation for the higher J_{SC} of the 5%-PEDOT device. As a result, the charge carrier lifetime of the 5%-PEDOT device is four times longer than that of the 100%-PEDOT device, which indicates that the 5%-PEDOT more efficiently transport holes while reducing carrier trapping and recombination. The ITO-only device shows low recombination resistance and high charge accumulation and result in the low charge extraction efficiency. The results of the impedance analysis clearly indicate that while the HTL is an essential layer in PSCs, only a very thin PEDOT layer is necessary to obtain the full benefit of the HTL.

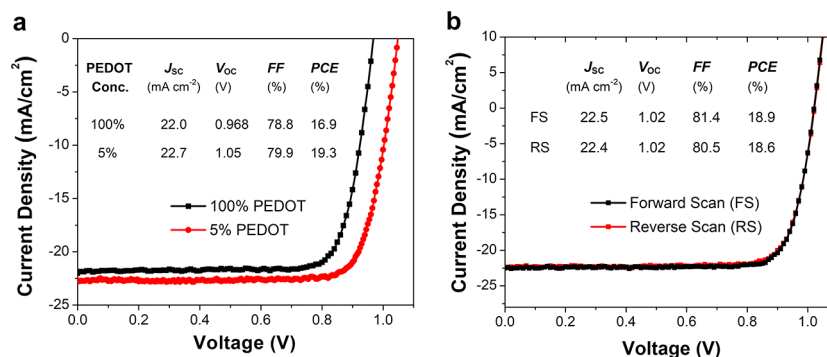


Figure 5. (a) J - V curves of the champion devices prepared with various substrates under nominal 1 sun illumination (0.988 sun actual) and (b) J - V curves recorded under reverse and forward scanning directions.

The effect of PEDOT thickness is also investigated by fitting the dark J - V characteristics Shockley diode equation. Figure 4c shows the dark J - V curves for the devices with varying concentration of PEDOT, which all fit well with the diode equation.³¹ The fitting parameters are summarized in Table S1. The ITO-only device shows the largest current leakage, which is over 1 order of magnitude higher than that of the 5%-PEDOT device. Though the 100%-PEDOT device shows a comparable diode ideality factor with the 5%-PEDOT devices, indicating similar bulk recombination, the large current leakage caused by charge recombination at the interfaces is likely a large contributor to the lower device PCE with the thicker PEDOT layer. In addition, the improved conductivity of the thinner PEDOT layers is also expected to contribute to the PCE enhancement (Figure 4d).²⁶

Figure 5a shows the J - V curve of champion devices with the 5%-PEDOT layer and the 100%-PEDOT layer, respectively. The 5%-PEDOT device shows a PCE of 19.3% with a J_{SC} of 22.7 mA cm⁻², a V_{OC} of 1.05 V, and an FF of 79.9%. In contrast, the best device on the 100%-PEDOT layer only yields a PCE up to 16.9%, with a J_{SC} of 22.0 mA cm⁻², a V_{OC} of 0.968 V, and an FF of 78.8%. The EQE spectrum of the device is shown in Figure S5 where the integrated photocurrent of the device is 22.1 mA cm⁻², which is consistent with the J_{SC} values obtained from J - V measurements. Moreover, the device exhibits negligible photocurrent hysteresis when measured with forward and reverse bias (Figure 5b), which again indicates that the device has efficient charge extraction on both sides of a high-quality perovskite film so that there is not an accumulation of space charge.³¹ We note that a previous report using a diluted PEDOT solution for the HTL resulted in good device performance, which is consistent with our results.³²

3. CONCLUSIONS

In summary, we have systematically investigated the significant effect that simple changes in PEDOT thickness can have on the performance of PSCs. The results indicate that an ultrathin PEDOT layer is beneficial to form homogenous and uniform perovskite films with a larger grain size, efficiently extract holes from perovskite film, lower the interface charge recombination, and lower photocurrent leakage. By moving from a 40 nm PEDOT layer to a 2 nm PEDOT layer, the device performance improved from 16.9% to 19.3% with photovoltages consistently above 1.0 V. This study not only provides a simple strategy to improve performance of PSCs but also could lower the cost of devices by reducing the need for expensive HTLs.

4. EXPERIMENTAL SECTION

4.1. Materials and Precursor Preparation. The following materials were used as received: anhydrous DMF (Sigma-Aldrich), anhydrous dimethyl sulfoxide (Sigma-Aldrich), methylammonium iodide (Lumtech), PbI₂ (Sigma-Aldrich), PbCl₂ (Sigma-Aldrich), C₆₀ (MER Corporation), 2,9-dimethyl-4,7-diphenyl-1,10-phenanthroline (BCP, Lumtech), and PEDOT (Clevios PVP AI 4083, 1.3 wt %, Heraeus). The PEDOT was diluted to various concentrations with deionized water.

The perovskite precursor solution was prepared with the procedure outlined in our previous report.³¹ The solutions were then stirred for 1 h and filtered with 0.45 μm polytetrafluoroethylene filters before use.

4.2. Device Fabrication. ITO substrates were spin-coated with PEDOT solutions at 6000 rpm for 10 s and then annealed at 120 °C for 10 min. The perovskite film was prepared with the procedure outlined in our previous report.³¹ The substrates were then coated with C₆₀ (20 nm), BCP (7.5 nm), and Ag (80 nm) in a thermal evaporation chamber at a base pressure of 3 × 10⁻⁶ Torr through a shadow mask with a device area (12.15 mm²) defined by the mask.

4.3. Measurement and Characterization. The thickness of the PEDOT film was measured by ellipsometry (Woollam Vase). The current-density-voltage characteristics (J - V curves) were measured with a Keithley 2420 source unit in the dark and under AM1.5 G solar simulation (xenon arc lamp with a spectral-mismatch factor of 0.988) with a scan rate of 50 mV/s. The light intensity was measured using a calibrated Si reference cell (NREL) with KG5 filter. EQE measurements were performed by using a monochromator to select wavelengths from a QTH lamp. The intensity at each wavelength was calibrated with a Si detector using a chopper and lock-in amplifier. A Bruker D2 phaser system was used to collect XRD data (Cu Kα, 0.154 nm). Impedance measurements were collected with an impedance analyzer (μAutolabIII FRA2) in the frequency range from 10⁵ to 0.01 Hz in logarithmic steps (dark, 0.6 V forward bias). All the device and structural measurements were collected on un-encapsulated devices/samples in air. SEM images were collected using a field-emission SEM (Carl Zeiss Auriga Dual Column FIB SEM).

■ ASSOCIATED CONTENT

Supporting Information

The Supporting Information is available free of charge on the ACS Publications website at DOI: 10.1021/acsomega.8b00741.

Transmittance spectra of PEDOT films, contact angle measurements, dark J - V curves of devices and fitted curves, the J - V curves of ITO/PEDOT/MoO₃ (20 nm)/Ag devices, and the corresponding EQE spectra of the champion devices prepared on the 5%-PEDOT layer (PDF)

AUTHOR INFORMATION

Corresponding Author

*E-mail: rlunt@msu.edu (R.R.L.).

ORCID

Qiong Wang: 0000-0002-5849-4352

Thomas W. Hamann: 0000-0001-6917-7494

Richard R. Lunt: 0000-0003-4248-6312

Present Addresses

^{||}Helmholtz-Zentrum Berlin für Materialien und Energie, Kekuléstraße 5, 12489 Berlin (Q.W.).

[†]Ubiquitous Energy Inc, Redwood City, CA 94063 (C.J.T.).

[#]Intel Corporation, Hillsboro, OR 97124 (M.Y.).

Notes

The authors declare no competing financial interest.

ACKNOWLEDGMENTS

The authors acknowledge the financial support from the Michigan State University Strategic Partnership Grant (SPG) (D.L.) and from the U.S. Department of Energy (DOE) Office of Science, Basic Energy Sciences (BES), under Award # DE-SC0010472 (structural and optical characterization) (P.C.).

REFERENCES

- (1) Kojima, A.; Teshima, K.; Shirai, Y.; Miyasaka, T. Organometal halide perovskites as visible-light sensitizers for photovoltaic cells. *J. Am. Chem. Soc.* **2009**, *131*, 6050–6051.
- (2) Zhou, H.; Chen, Q.; Li, G.; Luo, S.; Song, T.-b.; Duan, H.-S.; Hong, Z.; You, J.; Liu, Y.; Yang, Y. Interface engineering of highly efficient perovskite solar cells. *Science* **2014**, *345*, 542.
- (3) Tan, H.; Jain, A.; Voznyy, O.; Lan, X.; García de Arquer, F. P.; Fan, J. Z.; Quintero-Bermudez, R.; Yuan, M.; Zhang, B.; Zhao, Y.; Fan, F.; Li, P.; Quan, L. N.; Zhao, Y.; Lu, Z.-H.; Yang, Z.; Hoogland, S.; Sargent, E. H. Efficient and stable solution-processed planar perovskite solar cells via contact passivation. *Science* **2017**, *355*, 722–726.
- (4) Shin, S. S.; Yeom, E. J.; Yang, W. S.; Hur, S.; Kim, M. G.; Im, J.; Seo, J.; Noh, J. H.; Seok, S. I. Colloidally prepared La-doped BaSnO₃ electrodes for efficient, photostable perovskite solar cells. *Science* **2017**, *356*, 167–171.
- (5) Zheng, X.; Chen, B.; Dai, J.; Fang, Y.; Bai, Y.; Lin, Y.; Wei, H.; Zeng, X. C.; Huang, J. Defect passivation in hybrid perovskite solar cells using quaternary ammonium halide anions and cations. *Nat. Energy* **2017**, *2*, 17102.
- (6) Liu, M.; Johnston, M. B.; Snaith, H. J. Efficient planar heterojunction perovskite solar cells by vapour deposition. *Nature* **2013**, *501*, 395–398.
- (7) Burschka, J.; Pellet, N.; Moon, S.-J.; Humphry-Baker, R.; Gao, P.; Nazeeruddin, M. K.; Grätzel, M. Sequential deposition as a route to high-performance perovskite-sensitized solar cells. *Nature* **2013**, *499*, 316–319.
- (8) Yang, W. S.; Park, B.-W.; Jung, E. H.; Jeon, N. J.; Kim, Y. C.; Lee, D. U.; Shin, S. S.; Seo, J.; Kim, E. K.; Noh, J. H.; Seok, S. I. Iodide management in formamidinium-lead-halide-based perovskite layers for efficient solar cells. *Science* **2017**, *356*, 1376–1379.
- (9) Liu, D.; Kelly, T. L. Perovskite solar cells with a planar heterojunction structure prepared using room-temperature solution processing techniques. *Nat. Photonics* **2014**, *8*, 133–138.

(10) Jiang, Q.; Zhang, L.; Wang, H.; Yang, X.; Meng, J.; Liu, H.; Yin, Z.; Wu, J.; Zhang, X.; You, J. Enhanced electron extraction using SnO₂ for high-efficiency planar-structure HC(NH₂)₂PbI₃-based perovskite solar cells. *Nat. Energy* **2016**, *2*, 16177.

(11) Jeng, J.-Y.; Chiang, Y.-F.; Lee, M.-H.; Peng, S.-R.; Guo, T.-F.; Chen, P.; Wen, T.-C. CH₃NH₃PbI₃ perovskite/fullerene planar-heterojunction hybrid solar cells. *Adv. Mater.* **2013**, *25*, 3727–3732.

(12) Liu, D.; Yang, J.; Kelly, T. L. Compact layer free perovskite solar cells with 13.5% efficiency. *J. Am. Chem. Soc.* **2014**, *136*, 17116–17122.

(13) Bi, D.; Tress, W.; Dar, M. I.; Gao, P.; Luo, J.; Renevier, C.; Schenk, K.; Abate, A.; Giordano, F.; Correa Baena, J.-P.; Decoppet, J.-D.; Zakeeruddin, S. M.; Nazeeruddin, M. K.; Grätzel, M.; Hagfeldt, A. Efficient luminescent solar cells based on tailored mixed-cation perovskites. *Sci. Adv.* **2016**, *2*, No. e1501170.

(14) Noel, N. K.; Stranks, S. D.; Abate, A.; Wehrenfennig, C.; Guarnera, S.; Haghighirad, A.-A.; Sadhanala, A.; Eperon, G. E.; Pathak, S. K.; Johnston, M. B.; Petrozza, A.; Herz, L. M.; Snaith, H. J. Lead-free organic-inorganic tin halide perovskites for photovoltaic applications. *Energy Environ. Sci.* **2014**, *7*, 3061–3068.

(15) Hao, F.; Stoumpos, C. C.; Cao, D. H.; Chang, R. P. H.; Kanatzidis, M. G. Lead-free solid-state organic-inorganic halide perovskite solar cells. *Nat. Photonics* **2014**, *8*, 489–494.

(16) Pang, S.; Hu, H.; Zhang, J.; Lv, S.; Yu, Y.; Wei, F.; Qin, T.; Xu, H.; Liu, Z.; Cui, G. NH₂CH-NH₂PbI₃: An alternative organolead iodide perovskite sensitizer for mesoscopic solar cells. *Chem. Mater.* **2014**, *26*, 1485–1491.

(17) Mei, A.; Li, X.; Liu, L.; Ku, Z.; Liu, T.; Rong, Y.; Xu, M.; Hu, M.; Chen, J.; Yang, Y.; Grätzel, M.; Han, H. A hole-conductor-free, fully printable mesoscopic perovskite solar cell with high stability. *Science* **2014**, *345*, 295.

(18) Bi, D.; Yi, C.; Luo, J.; Decoppet, J.-D.; Zhang, F.; Zakeeruddin, S. M.; Li, X.; Hagfeldt, A.; Grätzel, M. Polymer-templated nucleation and crystal growth of perovskite films for solar cells with efficiency greater than 21%. *Nat. Energy* **2016**, *1*, 16142.

(19) Park, Y.; Berger, J.; Tang, Z.; Müller-Meskamp, L.; Lasagni, A. F.; Vandewal, K.; Leo, K. Flexible, light trapping substrates for organic photovoltaics. *Appl. Phys. Lett.* **2016**, *109*, 093301.

(20) Kim, Y. H.; Lee, J.; Hofmann, S.; Gather, M. C.; Müller-Meskamp, L.; Leo, K. Achieving high efficiency and improved stability in ITO-free transparent organic light-emitting diodes with conductive polymer electrodes. *Adv. Funct. Mater.* **2013**, *23*, 3763–3769.

(21) Docampo, P.; Ball, J. M.; Darwich, M.; Eperon, G. E.; Snaith, H. J. Efficient organometal trihalide perovskite planar-heterojunction solar cells on flexible polymer substrates. *Nat. Commun.* **2013**, *4*, 2761.

(22) Yan, W.; Ye, S.; Li, Y.; Sun, W.; Rao, H.; Liu, Z.; Bian, Z.; Huang, C. Hole-Transporting materials in inverted planar perovskite solar cells. *Adv. Energy Mater.* **2016**, *6*, 1600474.

(23) Chen, K.; Hu, Q.; Liu, T.; Zhao, L.; Luo, D.; Wu, J.; Zhang, Y.; Zhang, W.; Liu, F.; Russell, T. P.; Zhu, R.; Gong, Q. Charge-carrier balance for highly efficient inverted planar heterojunction perovskite solar cells. *Adv. Mater.* **2016**, *28*, 10718–10724.

(24) Wang, Q.; Chueh, C.-C.; Eslamian, M.; Jen, A. K.-Y. Modulation of PEDOT: PSS pH for efficient inverted perovskite solar cells with reduced potential loss and enhanced stability. *ACS Appl. Mater. Interfaces* **2016**, *8*, 32068–32076.

(25) Liu, H.; Li, X.; Zhang, L.; Hong, Q.; Tang, J.; Zhang, A.; Ma, C.-Q. Influence of the surface treatment of PEDOT: PSS layer with high boiling point solvent on the performance of inverted planar perovskite solar cells. *Org. Electron.* **2017**, *47*, 220–227.

(26) Zuo, C.; Ding, L. Modified PEDOT layer makes a 1.52 V Voc for perovskite/PCBM solar cells. *Adv. Energy Mater.* **2017**, *7*, 1601193.

(27) Peng, H.; Sun, W.; Li, Y.; Ye, S.; Rao, H.; Yan, W.; Zhou, H.; Bian, Z.; Huang, C. Solution processed inorganic V₂O₅ as interfacial function materials for inverted planar-heterojunction perovskite solar cells with enhanced efficiency. *Nano Res.* **2016**, *9*, 2960–2971.

(28) Giuri, A.; Masi, S.; Colella, S.; Kovtun, A.; Dell'Elce, S.; Treossi, E.; Liscio, A.; Corcione, C. E.; Rizzo, A.; Listorti, A. Cooperative effect of GO and glucose on PEDOT: PSS for high V_{OC} and hysteresis-free

solution-processed perovskite solar cells. *Adv. Funct. Mater.* **2016**, *26*, 6985–6994.

(29) Liu, D.; Traverse, C. J.; Chen, P.; Elinski, M.; Yang, C.; Wang, L.; Young, M.; Lunt, R. R. Aqueous-containing precursor solutions for efficient perovskite solar cells. *Adv. Sci.* **2018**, *5*, 1700484.

(30) Bi, C.; Wang, Q.; Shao, Y.; Yuan, Y.; Xiao, Z.; Huang, J. Non-wetting surface-driven high-aspect-ratio crystalline grain growth for efficient hybrid perovskite solar cells. *Nat. Commun.* **2015**, *6*, 7747.

(31) Liu, D.; Wang, Q.; Traverse, C. J.; Yang, C.; Young, M.; Kuttipillai, P. S.; Lunt, S. Y.; Hamann, T. W.; Lunt, R. R. Impact of ultrathin C_{60} on perovskite photovoltaic devices. *ACS Nano* **2018**, *12*, 876–883.

(32) Heo, J. H.; Han, H. J.; Kim, D.; Ahn, T. K.; Im, S. H. Hysteresis-less inverted $CH_3NH_3PbI_3$ planar perovskite hybrid solar cells with 18.1% power conversion efficiency. *Energy Environ. Sci.* **2015**, *8*, 1602–1608.